Published OnlineFirst April 14, 2009; DOI: 10.1158/0008-5472.CAN-08-3834

Research Article

Mathematical Oncology

Multiparameter Computational Modeling of Tumor Invasion

Elaine L. Bearer,[1,2] John S. Lowengrub,[3,4] Hermann B. Frieboes,[5] Yao-Li Chuang,[5] Fang Jin,[3] Steven M. Wise,[3,12] Mauro Ferrari,[6,7,8,10] David B. Agus,[13] and Vittorio Cristini[5,7,9,11]

[1]Department of Pathology and Laboratory Medicine, and Division of Engineering, Brown University, Providence, Rhode Island; [2]Department of Biology, California Institute of Technology, Pasadena, California; Departments of [3]Mathematics and [4]Biomedical Engineering, University of California, Irvine, California; [5]School of Health Information Sciences, [6]Division of Nanomedicine, and [7]Department of Biomedical Engineering, University of Texas Health Science Center; Departments of [8]Experimental Therapeutics and [9]Systems Biology, The University of Texas M. D. Anderson Cancer Center; [10]Department of Bioengineering, Rice University, Houston, Texas; [11]Department of Biomedical Engineering, The University of Texas, Austin, Texas; [12]Department of Mathematics, University of Tennessee, Knoxville, Tennessee; and [13]USC Center for Applied Molecular Medicine, University of Southern California, Los Angeles, California

Abstract

Clinical outcome prognostication in oncology is a guiding principle in therapeutic choice. A wealth of qualitative empirical evidence links disease progression with tumor morphology, histopathology, invasion, and associated molecular phenomena. However, the quantitative contribution of each of the known parameters in this progression remains elusive. Mathematical modeling can provide the capability to quantify the connection between variables governing growth, prognosis, and treatment outcome. By quantifying the link between the tumor boundary morphology and the invasive phenotype, this work provides a quantitative tool for the study of tumor progression and diagnostic/prognostic applications. This establishes a framework for monitoring system perturbation towards development of therapeutic strategies and correlation to clinical outcome for prognosis. [Cancer Res 2009;69(10):4493–501]

Major Findings

We apply a biologically founded, multiscale, mathematical model to identify and quantify tumor biologic and molecular properties relating to clinical and morphological phenotype and to demonstrate that tumor growth and invasion are predictable processes governed by biophysical laws, and regulated by heterogeneity in phenotypic, genotypic, and microenvironmental parameters. This heterogeneity drives migration and proliferation of more aggressive clones up cell substrate gradients within and beyond the central tumor mass, while often also inducing loss of cell adhesion. The model predicts that this process triggers a gross morphologic instability that leads to tumor invasion via individual cells, cell chains, strands, or detached clusters infiltrating into adjacent tissue producing the typical morphologic patterns seen, e.g., in the histopathology of glioblastoma multiforme. The model further predicts that these different morphologies of infiltration correspond to different stages of tumor progression regulated by heterogeneity.

Introduction

Prognosis of clinical outcome in oncology determines treatment decisions in patients with early and advanced cancer. Variables currently used include epidemiologic information, tumor type, molecular characterization, and clinical parameters such as tumor size and the presence of nodal and extranodal metastasis (tumor-node-metastasis staging). Quantitative histopathologic analysis is often limited to mitotic rates (number of mitoses per high-power field) and size and depth of invasive fingers (usually in microns). Degree of pleiomorphism and nuclear atypia are also used as prognosticators, although no quantitative definition has been generally accepted and hence this is often subjective to the pathologist. Animal models have been used to gain a molecular handle on which parameters indicate tumors with poor prognosis. New methodologies are needed to integrate and quantify these variables and enable the prediction of outcomes, selection of existing therapies, and development of new treatments, possibly on a personalized individual basis.

Correlations between morphology and cellular dynamics such as mitosis and motility are of fundamental importance here because these dynamics produce the various morphologies that generate the patterns pathologists use for diagnosis with proven diagnostic power. Morphologic analysis based on histopathology, though, is more art than science. Although pathologists describe different features in tumors, the relative effect of each feature on patient outcome and tumor progression remains unknown. To involve the epidemiology of human tumors, either in retrospective studies, which often exclude necessary data, or multi-year prospective studies, is cumbersome and time-consuming. Hence, determining the clinical predictive value from histologic epidemiology remains limited. Nevertheless, the value of histopathologic analysis is that it does not rely on any single feature alone and thus obtains a comprehensive view of the entire morphologic behavior of any particular tumor at the time of biopsy or excision.

Mathematical modeling can provide a rigorous, more precise approach for quantifying correlations between tumor parameters, prognosis, and treatment outcomes. The integration of these elements in a computational model of tumor progression would be an important tool to advance clinical decision-making. Tumors are complex systems dominated by large numbers of processes with highly nonlinear dynamics spanning a wide range of dimensions. Typically, such complex systems can be understood only through complementary experimental investigation and mathematical

Note: Supplementary data for this article are available at Cancer Research Online (http://cancerres.aacrjournals.org/).

Requests for reprints: Vittorio Cristini, University of Texas HSC-SHIS, 7000 Fannin no. 600, Houston, TX 77030. Phone: 713-500-3965; Fax: 713-500-3929; E-mail: vittorio.cristini@uth.tmc.edu.

doi:10.1158/0008-5472.CAN-08-3834

Published OnlineFirst April 14, 2009; DOI: 10.1158/0008-5472.CAN-08-3834

Quick Guide to Equations and Assumptions

Equation 1:

$$\phi\left(\frac{\partial\phi_i}{\partial t}+\nabla\cdot(\mathbf{u}_i\phi_i)\right)=-\nabla\cdot\mathbf{J}_{i,j}+S_i; i,j=1,2,3,4$$

This partial differential equation is derived from the conservation of mass (11, 12). The three-dimensional *in vivo* environment is modeled as a mixture of two viable tumor species (each with a volume fraction of ϕ_i, i = 1,2), dead tumor (ϕ_3) and host tissue (ϕ_4), and interstitial fluid (given indirectly by $\left(1-\sum_{i=1}^{4}\phi_i\right)$ and assumed to move freely) flowing through the ECM, which is treated as a porous medium. From left to right: change of volume fraction with respect to time; bulk transport by tumor mass with local velocity $\mathbf{u}_i$; fluxes $\mathbf{J}_i$ that account for mechanical interactions among cell species [based on a generalized Fick's Law (12)]; and net tissue source S_i from cell proliferation, death and mutation.

In Words: Temporal rate of change in a species at any tumor location equals the amount transported by the bulk tumor motion and cell adhesion, plus net result of mass creation/loss due to cell proliferation/death.

Major Assumptions

Tumor is a mixture of cells, interstitial fluid, and ECM. Cell adhesion is modeled through flux **J** using an approach from continuum thermodynamics (12).

Equation 2:

$$\mathbf{u}_i=-k(\phi_i)\left(\nabla p-\sum_l\gamma_l\frac{\delta E}{\delta\phi_l}\nabla\phi_l\right)+\chi_n(\phi_i,n)\nabla\frac{n}{n_V}+\chi_h(\phi_i,f)\nabla\frac{f}{f_H}; i=1,2,3,4$$

Cell velocity $\mathbf{u}_i$ of species i is a function of tissue oncotic (solid) pressure and cell mobility due to chemotaxis and haptotaxis. Right side: changes in pressure p create motion counteracted by cell adhesion γ_i mediated through an energy variation $\frac{\delta E}{\delta\phi_i}$ [for specific forms of this energy E and its variation, see ref. (12)]; chemotaxis χ_n due to soluble gradients of cell substrates and oxygen $n \le n_V$; haptotaxis χ_h due to insoluble gradients of ECM molecules $f \le f_H$. Motility k reflects cellular response to pressure gradients.

In Words: Species movement depends on oncotic pressure from cell proliferation, adhesion forces, and relative strengths of chemotaxis/haptotaxis.

Major Assumptions

Tumor is a viscous, inertialess fluid; interstitial fluid and cell motion through the ECM is similar to fluid flow in a porous medium. Cells move with a mass-averaged velocity arising from a generalized Darcy-type constitutive law for velocity from excess forces due to chemotaxis and haptotaxis. Cells prefer to adhere to one another rather than the host, modeled by the energy as a function of total solid tumor fraction. The tumor/host interface is well-delineated. Although the model is general, here total solid and liquid volume fractions are assumed constant. Therefore, separate fluid hydrostatic pressure and mechanical oncotic pressure due to cell-cell interactions are calculated. Energy E is a function of total tumor volume.

Equation 3:

$$S_1=\lambda_{M,1}\frac{n}{n_V}\phi_1-\lambda_{A,1}\phi_1-\lambda_N\mathcal{H}[n_N-n]\phi_1-\lambda_{TR}f_{\text{rand}}\phi_1,$$

$$S_2=\lambda_{TR}f_{\text{rand}}\phi_1+\lambda_{M,2}\frac{n}{n_V}\phi_2-\lambda_{A,2}\phi_2-\lambda_N\mathcal{H}[n_N-n]\phi_2.$$

Equations specify net sources of mass for two tumor viable species, directly linking Eq. 1 to the cell phenotype through hypothesized phenomenological functional relationships involving cell substrates (local oxygen or nutrient concentration n) through the tumor interstitium (12). For species S_1, right side terms represent, from left to right, volume fraction gained from mitosis (rate $\lambda_{M,1}$), and lost to apoptosis ($\lambda_{A,1}$), necrosis (λ_N), and mutation to become species S_2 (rate λ_{TR}). For species S_2, terms, respectively, represent gain in volume fraction from species S_1 through mutation (rate λ_{TR}) and mitosis ($\lambda_{M,2}$), and loss to apoptosis ($\lambda_{A,2}$) and necrosis (λ_N). Mutation rate λ_{TR} is a biased random function $0 \le f_{\text{rand}} \le 1$ of position and time within clone 1. Heaviside function $\mathcal{H}$, smoothed over a region of biologically realistic thickness (10–100 μm), models necrosis as a result of substrate depletion below a level n_N (11, 12, 10). Rates are inverse time.

In Words: The mass of original species increases through cell proliferation and decreases through apoptosis, necrosis, and mutation to the mutated species. The mass of mutated species increases through mitosis and mutation (from the original species), and decreases through apoptosis and necrosis.

Major Assumptions

Cells are composed entirely of water (12). Mitosis and necrosis are proportional to substrate concentration n (44). As mitosis occurs, an appropriate amount of water from the interstitial fluid is

modeling. Thus, there is a critical need for biologically realistic and predictive multiscale and multivariate models of tumor growth and invasion, and much recent effort has been directed towards this goal (1–7).

We previously described quantitative multiscale models (2, 8–13) to determine the precise functional relationships among quantifiable parameters from analyses of specific phenotypic or genetic alterations in a tumor, and from *in vitro* experiments (10) and clinical observations (2, 11) of tumor morphology such as cell arrangement patterns at the tumor boundary. These models predict that morphologic instability of a tumor mass, i.e., morphology resulting in "roughness" or harmonic content (14, 15) of the tumor margin, may provide a powerful tissue invasion mechanism because it allows tumor cells to escape the growth limitations imposed by diffusion (even *in vitro*; refs. 10, 16) and invade the host independently of the extent of angiogenesis (9, 10). Experiments with various glioma models *in vivo* (17–21) also support these findings. For example, recently published images of rat glioblastoma *in vivo* (20) showed that whereas the bulk tumor is perfused by blood, infiltrative cell clusters are much less perfused or not at all. These may be universal considerations that apply to tumor invasion across many different tissue types (22, 23).

Changes in tumor cells at the biochemical and genetic levels are also implicated in tumor progression. Mutations in genes that regulate cell cycle and adhesion result in unrestrained proliferation, invasion, and accumulation of further genetic damage characteristic of high-grade disease (24–26). In particular, in glioblastoma, the oncogene *EGFR* is frequently overexpressed, amplified, or mutated (27), and promotes mitosis (25), tumor progression *in vivo* (28), and inhibits apoptosis (29). See for example refs. (30–32) for recent

Published OnlineFirst April 14, 2009; DOI: 10.1158/0008-5472.CAN-08-3834

converted into the cell mass (12). Lysis represents a loss of solid mass converted into water that is absorbed into the interstitial fluid. Necrosis occurs only at sufficiently low nutrients.

Equation 4: $0 = D\nabla^2 n/n_V + \nu(1 - n/n_V)(1 - p/p_V)^+\delta_C - \eta_i\phi_i(n/n_V)$

This partial differential equation describes cell substrate concentration n across tumor tissue. Vessels originate randomly from existing vasculature (data not shown) around the growing tumor in response to vascular endothelial growth factor produced by hypoxic tissue. The first term on the right side models the diffusion of substrates n (with coefficient D) into tumor tissue, the second term represents the source of substrates at the vasculature denoted by δ_C as a function of distance from the vessels $(1 - n/n_V)$ and vascular pressure $(1 - p/p_V)$, and the third term represents uptake η_i by tumor species ϕ_i. Nutrient n is normalized with respect to the vasculature level n_V.

In Words: Steady-state cell substrate concentration across a tumor region equals the amount that diffuses into the region plus the production from the vasculature minus the amount uptaken by tumor cells.

Major assumptions

Nutrient diffusion occurs on a shorter time scale (minutes) than cell proliferation (days); hence, there is no time derivative on the left side, indicating a quasi-steady state.

mathematical models on the effect of *EGFR* gene expression on tumor growth patterns, and ref. (33) for phenomenological modeling of multiple mutations. The tumor suppressor genes *TP53* and *Rb* down-regulate cell division (25) and, secondarily affect oxygen/nutrient consumption, whereas *PTEN* controls angiogenesis, migration, and invasiveness (34). These genes are inactivated in most malignant brain tumors (35).

In the present study, we use a biologically founded, multiscale, mathematical model of tumor progression (8, 11–13) in three-dimensions (Supplemental Fig. S1) to show that molecular phenomena regulating cell proliferation, migration, and adhesion forces generate (including those associated with genetic evolution from lower-grade to higher-grade tumors), in a predictable and quantifiable way, heterogeneous proliferation and oxygen/nutrient demand (and suppression of apoptosis) across the three-dimensional tumor mass, determining its morphology. The model describes physical conservation laws (e.g., of mass and momentum), with conserved variables representing known characteristics of tumor behavior, and hypothesizes phenomenological functional relationships linking genetic and phenotypic effects, the microenvironment, and tissue-scale growth and morphology.

Variables that characterize the biophysics of tumor growth can be considered in the model, and applied to determine the probabilistic behavior of tumors given their molecular biology and pathologic appearance. By solving the model equations numerically, we predict the combination of variables most likely leading towards tumor invasiveness. At any given time during tumor growth, the model outputs the computed values of all relevant variables at every location within the three-dimensional tumor tissue, e.g., the spatial distributions of cell substrates and tumor cells. Rather than relying on one variable as the sole indicator, the multiparameter computational model enables a more systematic search to be performed for those values of specific variables that reproduce and explain observed tumor behavior. Variables include mutations and phenotypic changes affecting proliferation, apoptosis, nutrient uptake, tumor cell adhesion and motility, and their collective tumor mass effects. By quantitatively linking the invasive phenotype with the observable morphology of the tumor boundary, the model provides a tool for quantitative study of tumor progression as well as diagnostic and prognostic applications.

Materials and Methods

Histopathology of human glioma. Four archived autopsied brains (Brown University-Rhode Island Hospital Brain Bank) and 16 surgical specimens (Columbia University Brain Bank and Cooperative Human Tissue Network) were received according to institutional review board approval, and examined in H&E-stained paraffin sections prepared according to standard autopsy procedures. Diagnosis of glioblastoma multiforme was confirmed by two neuropathologists, and morphology at the tumor-brain interface imaged on a Zeiss AxioImager by standard bright-field and by fluorescence using FITC and rhodamine filters (11). Selective fluorescence in the rhodamine channel of hemoglobin in RBC combined with autofluorescence of connective tissue in the FITC channel greatly enhances the detection of vasculature patterns in H&E sections of archived material (11). Entire brain-tumor interface was imaged for each specimen, although many, especially the surgical specimens, were received in multiple fragments. Even in the autopsied brains, the tumor rendered the tissue friable, making it difficult to embed as a block. Representative images were selected for presentation here as comparison to model predictions. All patterns present in the group of tumors were included.

Multiscale tumor model. The model considers genotype, phenotype, and morphologic parameters (Quick Guide, Supplementary Data), and accounts for feedback from the microenvironment, i.e., mutations or phenotypic changes induced by hypoxia (36), as local levels of oxygen/nutrients induce changes in the mutation function. The model also allows

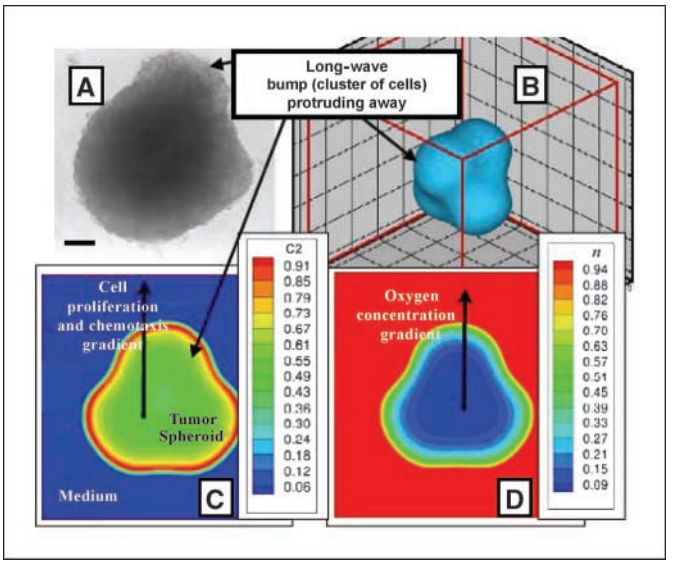

Figure 1. Onset of morphologic instability in glioblastoma is consistently replicated by the mathematical model. Collective motion of cells of clone 2 (*C2*; $\mathcal{M} = \{0,1\}$) is shown due to heterogeneous proliferation (and possibly chemotaxis) up concentration gradients and under weak cell adhesion ($\gamma_2 < 6.7_{M,2}$; Supplementary Data). *A, in vitro* glioblastoma spheroid (*bar,* 130 μm), and (*B–D*) computer simulation. Adapted from Frieboes et al. (10); reprinted with permission from the American Association for Cancer Research. *B,* representation of observed tumor shape; *C,* local mass fraction "C2" of viable tumor cells; and *D,* oxygen concentration "*n*" ($n = 1$ in the medium). Note hypoxic core (*D*) and corresponding low cell viability levels (*C*) within, and high viability at outer rim.

Published OnlineFirst April 14, 2009; DOI: 10.1158/0008-5472.CAN-08-3834

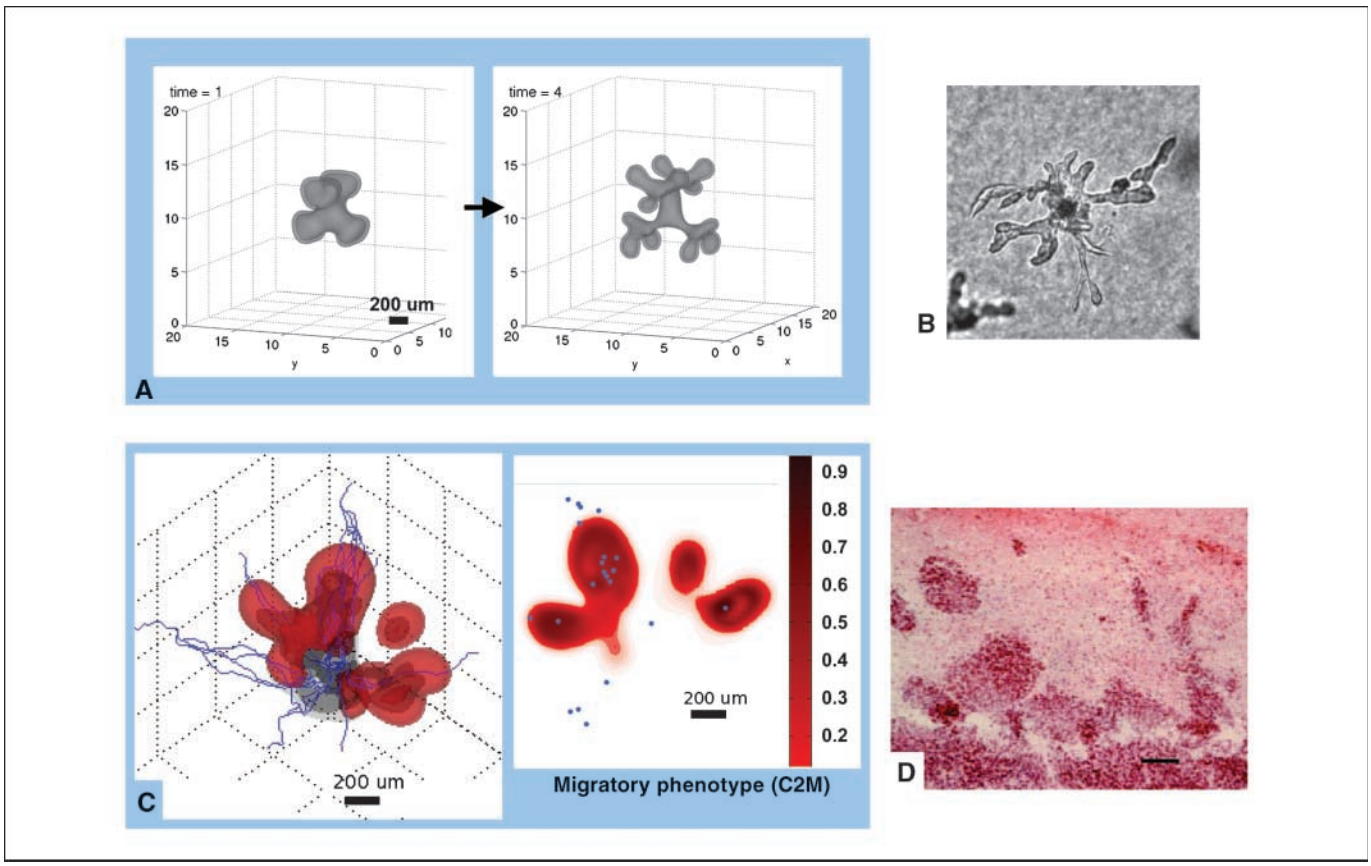

Figure 2. Variability and persistence of morphologic patterns predicted by the mathematical model simulating heterogeneity *in vitro* (*A*; refs. 10, 40) and *in vivo* (*C*; refs. 11, 12). In both cases, only the higher-grade clone 2 is simulated (no mutations), although the clone is allowed to acquire a hypoxia-induced migratory phenotype (Supplementary Data). *A,* proliferation is down-regulated and the clone migrates up oxygen gradients towards the far-field boundary (computational box not shown; *arrow,* time direction). *C,* migratory phenotype of tumor clone 2 (*C2M, red*); and the less motile clone 2 (*C2, gray*). Proliferation of both clones is regulated by oxygen levels. The darker interior region of the three-dimensional graph denotes necrotic region. Two-dimensional horizontal slice shows the distribution of C2M; small blue circles indicate the positions of mature, blood-conducting vessels. Morphologic instability occurs in both simulations because this clone's cell adhesion is low, resulting in cell strands in *A*, and fingers and detached clusters in *C*. Simulations are supported by experimental observations revealing morphologic instability after inducing hypoxia in spheroids *in vitro* [*B*; reprinted from Pennacchietti et al. (16), with permission from Elsevier] and in xenografts *in vivo* [*D*; *bar,* 80 μm; adapted from Rubenstein et al. (17), copyright Neoplasia].

for the development of a (hypoxia-induced) migratory phenotype. At the tumor scale, the model is based on first principles describing conservation laws of mass and momentum. Local mass fractions of tumor clones, necrotic, and host tissues are described. Phenomenological parameters describe cell adhesion. Tumor cell migration velocity depends on proliferation-driven mechanical pressure in the tissue, chemotaxis, and haptotaxis due to gradients of chemokines. Cell substrate delivery from the neovasculature (via convection and diffusion; refs. 8, 11, 37) and cellular uptake, and nutrient/oxygen diffusion through tumor tissue (refs. 8, 12) are modeled. The effects of each parameter on outcome can be tested individually or in combination.

Results

Figure 1 shows the onset of diffusion-driven morphologic instability (9, 10, 14, 15) from our simulations. Perturbations arise in the spatial arrangement of cells at the periphery of human glioma spheroids in culture (Fig. 1*A*) and are consistently replicated by our model (Fig. 1*B*). Once this asymmetrical shape is created, local cell substrate gradients (Fig. 1*D*) cause spatially heterogeneous cell proliferation and migration (Fig. 1*C*), as cells that are exposed to more substrates proliferate more. Mechanical forces, e.g., cell-cell and cell-matrix adhesion (which are, in general, stabilizing; refs. 10, 14, 22), were in this case not strong enough to prevent morphologic instability.

When the instability persists, it leads to the proliferative growth of bud-like clusters or "bumps" of cells (Figs. 1 and 2). *In vitro*, these eventually may detach as subspheroids from the parent spheroid (10), analogous to microsatellites *in vivo*, and also represent the initial stage of the growth of cell chains, strands, or detached clusters (2, 22) observed *in vitro* and *in vivo* (Fig. 2*B* and *D*). Simulations reveal that when chemotaxis or haptotaxis are dominant, e.g., if mitosis is down-regulated, protrusions begin as high-frequency perturbations (linear stability[8] predicts the growth of short wavelengths; refs. 13, 14) on the tumor surface and develop into cell chains and strands (ref. 22; Fig. 2*A*). When proliferation is the prevailing proinvasion mechanism, the buds grow into round fingers (Fig. 1*B*), which may detach as clusters (ref. 10; linear stability predicts the growth of long wavelength perturbations; refs. 9, 14, 15). This is clearly seen in Fig. 2*C*, in which cells acquire a hypoxia-induced migratory phenotype. These simulations are

[8] Linear stability analysis can be used to determine analytically how infinitesimal perturbations evolve at the tumor surface in time, as illustrated in refs. 9, 13–15.

Published OnlineFirst April 14, 2009; DOI: 10.1158/0008-5472.CAN-08-3834

supported by experimental observations under hypoxic conditions (Fig. 2*B* and *D*; refs. 16, 17).

As necrosis and substrate gradients develop within the tumor, proliferation may be down-regulated and motility up-regulated. Although various substrate components (e.g., oxygen, glucose, growth factors, and metabolites) may be determinants of these phenotypic changes, we focus on oxygen because of its well-established role in regulating cell proliferation and motility (e.g., ref. 16). Figure 3 shows a migratory or hypoxic growth stage, where palisading cells forming "Indian files" are seen from simulations (*A* and *B*) and from histology (*C* and *D*). In the simulations (hybrid continuum-discrete approach; Supplementary Data), individual cells originate in the perinecrotic region (center) and have undergone the phenotypic changes described above. In particular, the cells down-regulate proliferation and migrate via chemotaxis up oxygen gradients and haptotaxis up bound chemokines in the extracellular matrix (ECM), which the cells also degrade and remodel. The resulting morphology (Fig. 3*A* and *B*) compares with pathology data surprisingly well (Fig. 3*C* and *D*; see also ref. 11). As strands of cells move away from the perinecrotic regions and into the brain stroma, they may trigger angiogenesis, a wound-healing process, thereby increasing nutrient availability in the microenvironment. Increased oxygen and nutrients would result in the up-regulation of proliferation and down-regulation of motility, creating the microsatellite cell clusters in Fig. 2*D* (mouse brain) and Fig. 5*B* (human specimen, below).

Computer simulation of a human glioma over time in the proliferative growth stage produces finger-like extensions (Fig. 4). Expression of oncogenes and the absence of tumor suppressor pathways initially results in the net growth of a relatively low-grade type of morphology. After 2 months, the tumor expands to ~3 mm by co-opting the vasculature (which is not shown) while retaining a compact shape with negligible necrosis (Fig. 4*A*). However, increased nutrient demand generates hypoxic and other substrate gradients pointing radially outwards from the lesion (data not shown). A second, more proliferative clone, is generated by ongoing hypoxia-driven (36) mutations and starts to grow (*bottom left corner, shaded area*). Its higher cellular uptake introduces perturbations in the spatial gradients of oxygen, further enhancing local hypoxia. These gradients generate spatially heterogeneous cell proliferation and migration. After 4 months, this perturbation triggers a morphologic instability, which noticeably deforms the tumor mass (*bottom left*).

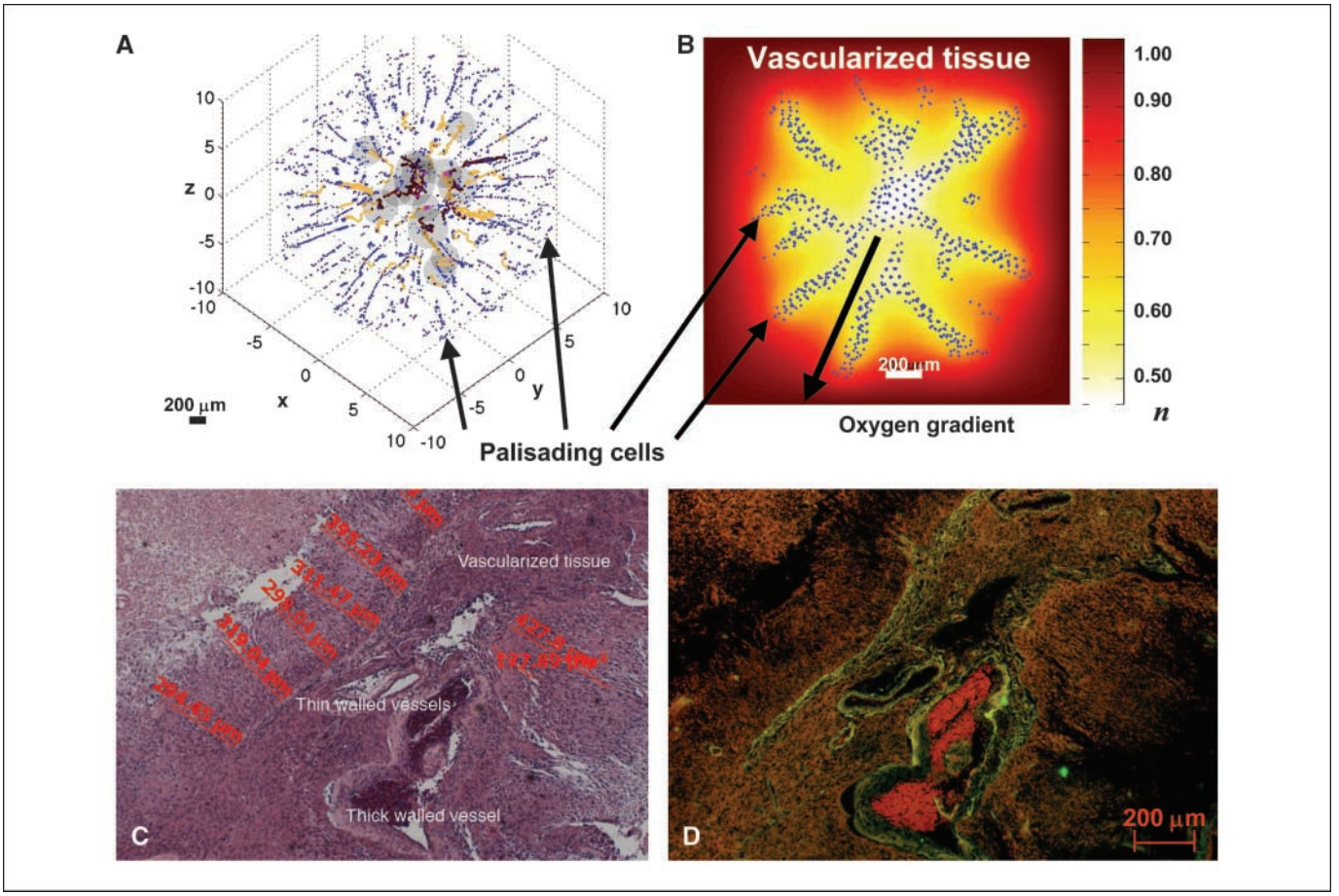

Figure 3. Palisading glial cells invade vascularized tissue as predicted by the model (*A* and *B*) and as observed in histology (*C* and *D*). *A,* computer simulation showing palisading cells escaping from the perinecrotic region (*dark gray*) by undergoing a hypoxia-induced phenotypic change to up-regulate motility and down-regulate adhesion and proliferation. Cell migration occurs via chemotaxis and haptotaxis in response to gradients of oxygen and ECM concentration, respectively (Materials and Methods). *Brown,* conducting vessels; *yellow,* nonconducting. *B,* background shows distribution of oxygen concentration ("*n*" in legend). $n = 1$ in vascularized tissue and is lower in the tumor (*white/yellow,* perinecrotic region). *C,* 4× magnification of a high-grade glioblastoma interior. *D,* corresponding fluorescent image showing vessels (*green* and *red*). As predicted by the simulations (*A* and *B*), palisading malignant glial cells (*C*) invade the vascularized tissue (*D*), amidst a tangle of thick-walled and thin-walled large vessels and a few smaller vessels from two areas of necrosis. Also, note the distances between necrosis and vessels (*C*), corroborating our choice for diffusion penetration length L_2 (Supplementary Data). Further phenotypic changes (e.g., down-regulation of motility and up-regulation of proliferation) may occur when migrating cells reach tissue regions richer in substrates, leading to the morphologies described in Figs. 4*D* and 5*A–D*.

Published OnlineFirst April 14, 2009; DOI: 10.1158/0008-5472.CAN-08-3834

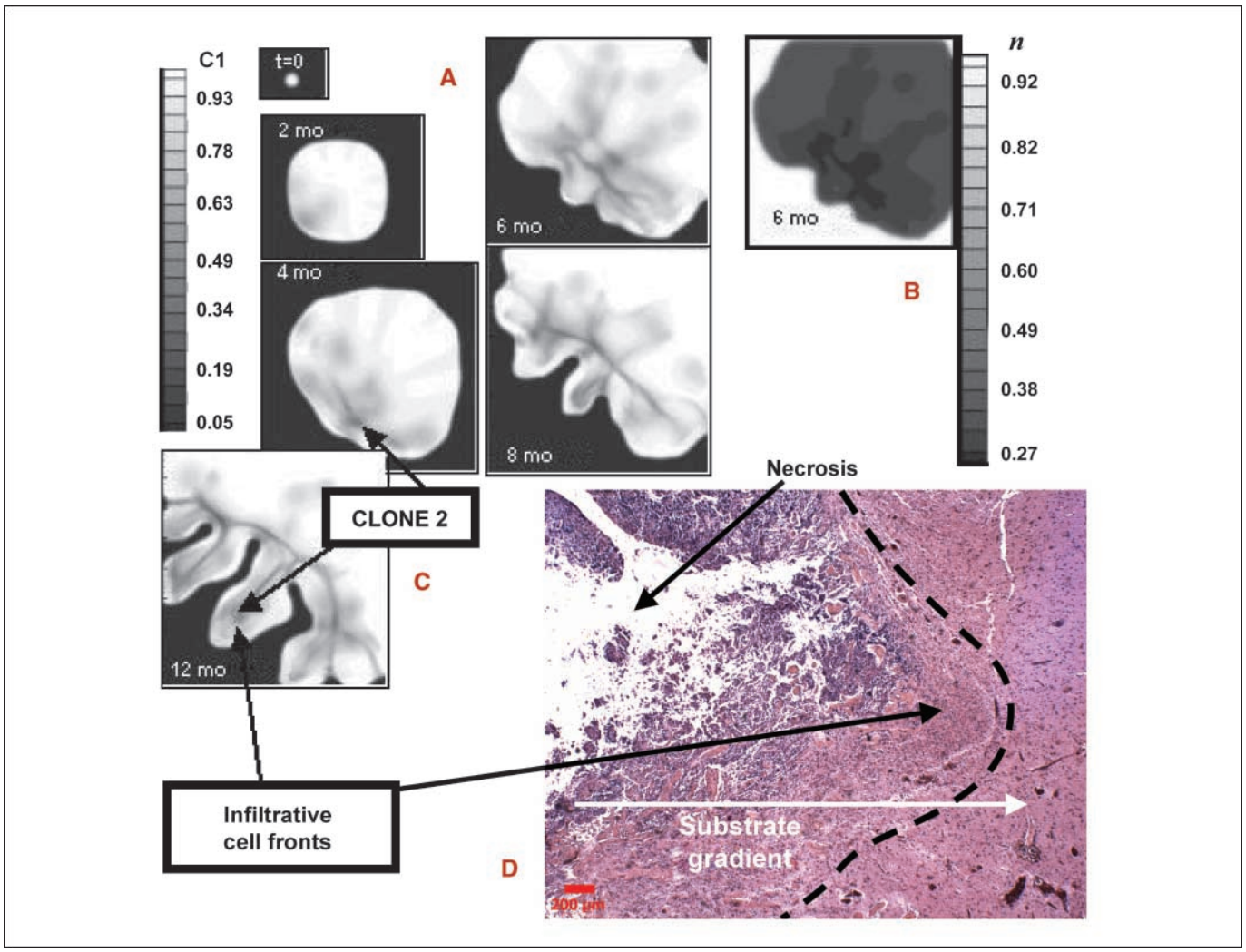

Figure 4. Infiltration of a high-grade glioma. *A,* computer simulation in proliferative growth stage (field of view = 6–10 mm). For each time snapshot, two-dimensional slices depict spatial distribution of two different clones: genotype $\mathcal{M}$ = {1,0} (lower-grade clone 1, "C1") evolving to $\mathcal{M}$ = {0,1} (higher-grade clone 2, "C2" = 1-C1; Materials and Methods). Legend: local mass fraction of C1. Arrows pointing to darker areas in the tumor indicate C2. *B,* simulated oxygen concentration ("*n*" in legend) at 6 mo, indicating hypoxic gradients (n = 1 in normal brain and is lower in tumor). The larger oxygen uptake of C2 enhances local hypoxia (e.g., *bottom left tumor corner*), and leads to shape instability in which clusters of C2 cells protrude "finger-like" into the tumor mass of C1 first, and in the host brain later. The model predicts that C2 expansion is the main determinant of tumor morphology. *C,* tumor detail at 12 mo showing invading fingers. *D,* histology section of a tumor front (*left*) showing an invading finger into more normal brain (*bar,* 200 μm). Normal brain (white matter) has fewer cell bodies and a more abundant amorphous matrix (*right*). Invading malignant astrocytes (*left*) have pleiomorphic nuclei and an irregular distribution. Note the clearly demarcated margin (*left of the dashed line*) between tumor and more normal brain. Neovascularization (and inflammation) at the tumor-brain interface is visible as darker spots (*to the right*) in brain parenchyma, implying that substrate gradients drive collective tumor cell infiltration into the brain. Morphology and size of the invading finger are consistent with simulation predictions (*A* and *B*), suggesting the proliferative growth stage.

Hypoxia and necrosis are present within the regions in which the more malignant clone grows. Shape instability leads to clusters of clone 2 protruding "finger-like" (darker) regions into the mass of clone 1 first, and the host brain later, growing at the expense of the less proliferative clone and the host tissue. We have also observed that detachment of these clusters may occur in our model (Fig. 2*C*; ref. 10). These fingers grow away from the bulk tumor and tend to follow substrate gradients.

In ~6 months' time, the aggressive, invasive proliferation of clone 2 (darker regions) enables it to infiltrate almost all regions of the tumor, in particular around the boundary, and leads to a higher-grade lesion. A bud-like protrusion emerges on the tumor (*bottom left*). Hypoxic, necrotic areas continue to expand (Fig. 4*B*). In 8 months, the glioma aggressively infiltrates the surrounding brain tissue. Clone 1 is being confined by competition with clone 2. Extensive necrosis is present. Additional buds have appeared, and the initial (*middle*) bud has grown into an invasive finger. Strands and clusters of clone 2 drive the growth of the finger and buds (extent of the darker area). Clone 1 has been mostly eliminated from this region of the tumor, and remains stagnant. In 12 months, the surrounding brain has been severely compromised. Expansion of clone 2, accompanied by continued necrosis, is now the main determinant of tumor morphology. The lesion reaches a size of ~4 cm in a little over 1 year of simulated time, consistent with human glioma progression (Fig. 4*C* shows only a tumor portion at 1 year).

Different tumors are likely to have different genomic instability factors—different types and mutation rates. The idealized tumor in Fig. 4*A–C* is "programmed" to exhibit the progressive appearance of one highly malignant clone (clone 2). In reality, multiple clones may arise with varying degrees of malignancy.

Published OnlineFirst April 14, 2009; DOI: 10.1158/0008-5472.CAN-08-3834

A histology section of glioblastoma from one patient reveals the tip of a round invading finger (Fig. 4*D*), consistent with the morphology and size of these infiltrative cell clusters predicted by simulations during the proliferative growth stage (Fig. 4*C* at 12 months, in which the tip of one protruding cell front is ~2 mm in size). The fact that tumor cells rely on vessels beyond the protrusions—and may grow towards blood vessels that they stimulate (11, 38, 39)—also suggests a proliferative growth stage because these vessels increase substrate availability in the microenvironment. Older tumor vessels may have thicker walls that are not as permeable for nutrient/oxygen exchange, and may become occluded due to increased pressure from the tumor mass (Supplementary Data), further promoting substrate gradients.

Additional histology sections from four glioblastomas (Fig. 5) reveal protruding fronts of cells pointing away from a necrotic area into an area of the host brain where neovascularization is evident. These invading fronts are also consistent with the tumor boundary morphology predicted by simulation in the proliferative growth regime (Fig. 4*A–C*). Although infiltrative shapes were consistently observed in histologic sections (Supplementary Data), the model predicts that their size may vary based on the stage of growth. For example, these shapes can be extremely slender in the hypoxic growth regime, down to single rows of palisading cells migrating up substrate concentration gradients (Fig. 3*A* and *B*), and thus, away from hypoxic regions, as seen in histology (Fig. 3*C* and *D*).

Supplemental Fig. S2 reports additional histologies showing invasive fingering. Such morphologies are predicted by the model to occur in the proliferative growth stage, in which there is increased substrate availability. This is confirmed by the presence of viable vessels in the histopathology acting as sources of substrates around the invasive fingers.

Discussion

We have used a biologically founded, mathematical model to show that tumor progression can be described as a predictable process dependent on biophysical laws. Conservation laws were posed with variables that account for genetic and phenotypic changes that influence cell proliferation, apoptosis, adhesion, motility, and uptake of substrates. Quantitative functional relationships were hypothesized linking genetic and phenotypic effects, the microenvironment, and tissue scale growth and morphology. Although the model was trained with *in vitro, in vivo*, and clinical data for glioma, these considerations may also apply to tumor

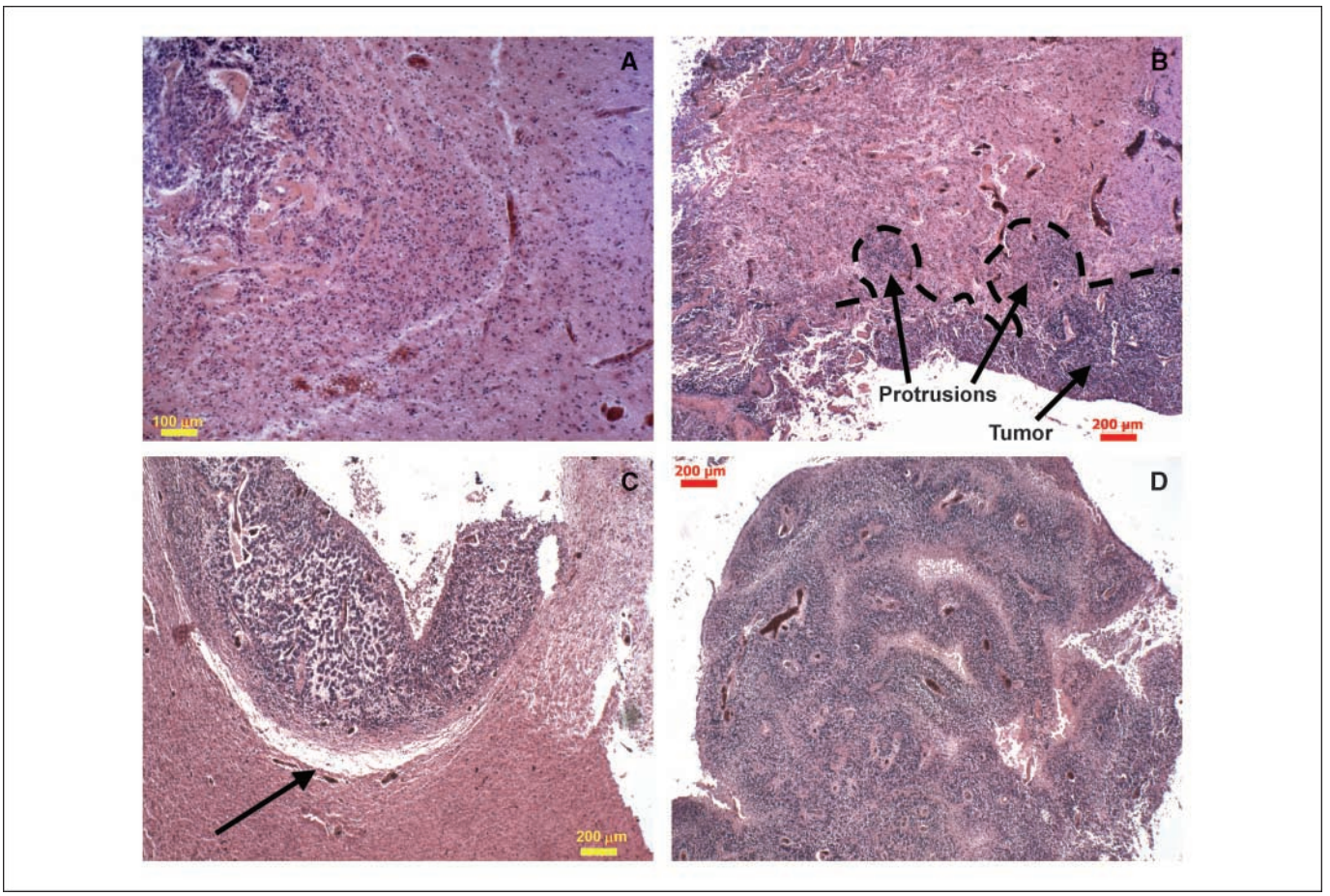

Figure 5. Histologic sections reveal infiltrative patterns predicted by simulations in the proliferative growth stage. *A,* higher magnification of invading finger shown in Fig. 4*D* [adapted from Frieboes et al. (11), with permission from Elsevier]. *B,* two invasive protrusions are seen emanating from the tumor mass. *C,* boundary of another protrusion from a different specimen is indicated (*arrow*); there also seems to be ECM degradation. *D,* morphology details of one large bulb-shaped tumor protrusion from *B* [reprinted from Frieboes et al. (11), with permission from Elsevier]. The interior reveals clusters of viable cells surrounding blood vessels, and areas depleted of cells farther away, indicating increased substrate availability in the microenvironment. Additional histology sections reveal similar features (Supplementary Data). Altogether, these data suggest the proliferative growth stage predicted by the model for this invading morphology.

Published OnlineFirst April 14, 2009; DOI: 10.1158/0008-5472.CAN-08-3834

invasion beyond glioma (22, 23). All known forms of collective cell migration (chains, strands, and detached clusters; ref. 22) observed in experiments and histopathology were consistently reproduced by the mathematical model (e.g., refs. 2, 10–14) for different values of the molecular and microenvironmental parameters, with heterogeneity in cellular genotype, phenotype, and the microenvironment being the regulating feature. Multiclonality, abnormal angiogenesis, or hypoxia-inducing local injuries, and even therapeutic intervention such as antiangiogenic therapy (9, 10, 17–19) could be the sources of this heterogeneity.

The central finding of this work is that tumor growth and invasion are not erratic or unpredictable, or solely explained through genomic and molecular events, but rather are predictable processes obeying biophysical laws, driven by microenvironmental substrate gradients, and regulated by genotypic, phenotypic, and microenvironmental parameters (e.g., cell adhesion, proliferation, and motility). The model enables quantitative study of invading cell clusters as functional units that move as complex systems. Substrate gradients, e.g., of nutrient, oxygen, growth factors, and metabolites, result from diffusion, cellular activity, and heterogeneous delivery and removal. This leads to local hypoxia, nutrient starvation, acidosis, necrosis, and the pleiomorphic appearance of tumors. The underlying physical mechanism of collective cell migration, i.e., a gross tumor morphologic instability (2, 8–10, 12–14, 40), maximizes cell exposure to substrates by evading a compact, nearly spherical morphology in favor of infiltrating shapes moving up gradients of substrates such as oxygen. Phenotypic changes that increase nutrient uptake and augment cell proliferation (and also increase cell motility and reduce adhesion) have a quantifiable effect on morphology at the tumor scale. In particular, they trigger invasive fingering into host tissue while inducing necrosis and angiogenesis for certain parameter conditions.

The model predicts that different morphologies of infiltration are associated with phenotypic and genotypic changes, which depend on cell substrate gradients and microenvironmental parameters, and reflect the growth stage of the tumor. In regions of hypoxia, these changes include the down-regulation of proliferation and up-regulation of motility, which under low cell adhesion results in palisading cells forming "Indian files" (Fig. 3*A* and *B*). As cells localize in tissue regions that are richer in substrates, i.e., better vascularized, further phenotypic changes occur in which motility is down-regulated and proliferation is up-regulated. This leads to the formation of wave-like patterns of cell rearrangements at the tumor boundary and round infiltrative fingers that can detach from the tumor bulk as clusters (Fig. 4*A*–*C*). Actually, different tumor regions may exhibit different growth regimes at the same time depending on heterogeneity in the local microenvironment and in cell genotypes/phenotypes. In our simulations, proliferation and collective migration of more aggressive clones or phenotypes drives tumor infiltration, as observed in patient biopsies (e.g., refs. 41, 42, and this study).

Model predictions of infiltrative morphologies in the hypoxic and proliferative growth stages compare well with the histopathology of human glioblastoma. Tumor microenvironment conditions were similar to those predicted in the model with respect to vascular distribution, implied cell substrate availability, and palisading of malignant cells between vascular and avascular regions. These findings are further supported by published correlations of invasion with hypoxia and necrosis induced in glioma by characteristically abnormal, inadequate, and hemorrhagic vasculature or by antiangiogenic therapy (17, 18, 36, 43, 44). A formal comparison between observations and model predictions, e.g., measured via a "merit function," could be performed as the next stage to confirm the model hypotheses.

By quantifying the close connection between the observable morphology of the tumor boundary and cellular/molecular dynamics, the work presented here provides a quantitative tool for the study of tumor progression and diagnostic/prognostic applications. This connection is important because the dynamics that give rise to various tumor morphologies also control invasiveness. In particular, by describing morphology as a function of parameters dependent on cellular and environmental phenomena (45, 46), the model quantifies, under the unifying umbrella of morphologic stability analyses, the often seemingly diverse and unrelated morphologies and invasive phenotypes, e.g., palisading cells, round fingers, and clusters. It is generally observed (22) that premetastatic phenotypic transitions (e.g., epithelial-mesenchymal transitions) follow a collective migration stage, and are regulated by the environment (e.g., local hypoxia; refs. 45, 46). Invasive characteristics may strongly influence whether a tumor can be effectively treated by local resection and may suggest specific treatment options (1, 33, 47). Observation of tumor morphology, for example, could indicate the presence of hypoxia, and therefore, the potential to respond to oxygen-dependent treatments such as radiation therapy and certain chemotherapy treatments.

The model may be used to study system perturbations by therapeutic intervention and may aid in the design of novel clinical end points in therapeutic trials. By integrating the model with patient data for key tumor phenotypic and microenvironmental parameters (2), model results could be used to enhance clinical outcome prognostication. Initial conditions regarding tumor physical location, structure, and vasculature, e.g., obtained from contrast-enhanced magnetic resonance imaging and possibly coupled with computed tomograpy would be translated using a computer program to the model coordinate system (2), e.g., a finite-element computational mesh discretizing the space occupied by tumor and host tissues (12). Viable region spatial information and microvasculature structure would be obtained from histopathology (11). Vasculature-specific information could be defined from dynamic contrast–enhanced computed tomograpy, yielding blood volume, flow, and microvascular permeability parameters (2). Other input data include cell scale parameters (e.g., proliferation rates). The model then calculates local tumor growth, angiogenesis, and response to treatment under various conditions by solving in time and space the conservation and other equations at the tissue scale.

The model allows predictions of cellular and molecular perturbations that may alter invasiveness and that can be measured through changes in tumor morphology. Therefore, morphologies obtained from the model could be used to both understand the underlying cellular physiology and predict subsequent invasive behavior. For example, novel individualized therapeutic strategies could be designed in which microenvironmental and cellular factors are manipulated to decrease invasiveness and promote well-defined tumor margins—an outcome that would also benefit treatment by improving local tumor control through surgery or radiation. In addition to existing strategies that act on relevant cellular behaviors (e.g., promotion of tumor cell adhesiveness; refs. 10, 14, 22), or that target oncogenes such as *EGFR*, tumor morphologic stability could be enhanced by improving nutrient supply (9, 40), thus enforcing a more homogeneous microenvironment and normoxic conditions. This could be achieved through "vascular normalization" (9, 48) or uniform nanoparticle delivery (49), e.g., releasing oxygen and

antiangiogenic drugs. Furthermore, by maintaining microenvironmental homogeneity, effects of genetic mutations that lead to morphologic instability may be minimized (e.g., ref. 50), without direct intervention at the genotype level.

Applying biologically founded, mathematical modeling to quantify the connections between the microenvironment, tumor morphology, genotype, and phenotype may direct prognosis beyond the limitations of current methodologies, and suggest new directions in the way we think about cancer growth and invasion.

Disclosure of Potential Conflicts of Interest

No potential conflicts of interest were disclosed.

Acknowledgments

Received 10/7/08; revised 3/23/09; accepted 3/27/09; published OnlineFirst 4/14/09.

Grant support: The Cullen Trust of Health Care, NSF-DMS 0818104, National Cancer Institute, Department of Defense (V. Cristini); NSF Division of Mathematical Sciences and NIH-P50GM76516 for a Center of Excellence in Systems Biology at University of California, Irvine (J.S. Lowengrub); NIGMS-GM47368 and NINDS-NS046810 (E.L. Bearer); and NCI U54 Center for Cancer Nanotechnology Excellence-TR CA119367 (D.B. Agus).

The costs of publication of this article were defrayed in part by the payment of page charges. This article must therefore be hereby marked *advertisement* in accordance with 18 U.S.C. Section 1734 solely to indicate this fact.

We acknowledge Robert Gatenby (Moffitt Cancer Center) for useful discussions, Xiangrong Li (UC-Irvine) for Fig. 2*A*, Ed Stopa and the Pathology Department (Rhode Island Hospital) for autopsied specimens, Aleksey Novikov and Bryan Kinney (E.L. Bearer's lab) for technical assistance, and Henry Hirschberg (UC-Irvine) for information about recent results (20).

References

1. Sanga S, et al. Mathematical modeling of cancer progression and response to chemotherapy. Expert Rev Anticancer Ther 2006;6:1361–76.
2. Sanga S, et al. Predictive oncology: a review of multidisciplinary, multiscale in silico modeling linking phenotype, morphology and growth. Neuroimage 2007; 37:S120–34.
3. Araujo R, McElwain D. A history of the study of solid tumour growth: the contribution of mathematical modelling. Bull Math Biol 2004;66:1039–91.
4. Hatzikirou H, Deutsch A, Schaller C, Simon M, Swanson K. Mathematical modeling of glioblastoma tumour development: a review. Math Models Methods Appl Sci 2005;15:1779–94.
5. Byrne HM, Alarćon T, Owen MR, Webb SW, Maini PK. Modeling aspects of cancer dynamics: a review. Philos Trans R Soc A 2006;364:1563–78.
6. Roose T, Chapman SJ, Maini PK. Mathematical models of avascular tumor growth. SIAM Review 2007;49:179–208.
7. Anderson ARA, Quaranta V. Integrative mathematical oncology. Nat Rev Cancer 2008;8:227–44.
8. Zheng X, Wise SM, Cristini V. Nonlinear simulation of tumor necrosis, neo-vascularization and tissue invasion via an adaptive finite-element/level-set method. Bull Math Biol 2005;67:211–59.
9. Cristini V, et al. Morphologic instability and cancer invasion. Clin Cancer Res 2005;11:6772–9.
10. Frieboes HB, et al. An integrated computational/experimental model of tumor invasion. Cancer Res 2006; 66:1597–604.
11. Frieboes HB, et al. Computer simulation of glioma growth and morphology. Neuroimage 2007;37:S59–70.
12. Wise SM, Lowengrub JS, Frieboes HB, Cristini C. Three-dimensional multispecies nonlinear tumor growth. I. Model and numerical method. J Theor Biol 2008;253:524–43.
13. Cristini V, Li X, Lowengrub JS, Wise SM. Nonlinear simulations of solid tumor growth using a mixture model: invasion and branching. J Math Biol 2009;58:723–63.
14. Cristini V, Lowengrub J, Nie Q. Nonlinear simulation of tumor growth. J Math Biol 2003;46:191–224.
15. Li,X, Cristini V, Nie Q, Lowengrub JS. Nonlinear three-dimensional simulation of solid tumor growth. Discrete Contin Dyn Syst B 2007;7:581–604.
16. Pennacchietti S, Michieli P, Galluzzo M, Giordano S, Comoglio P. Hypoxia promotes invasive growth by transcriptional activation of the met protooncogene. Cancer Cell 2003;3:347–61.
17. Rubenstein JL, et al. Anti-VEGF antibody treatment of glioblastoma prolongs survival but results in increased vascular cooption. Neoplasia 2000;2:306–14.
18. Kunkel P, et al. Inhibition of glioma angiogenesis and growth *in vivo* by systemic treatment with a monoclonal antibody against vascular endothelial growth factor receptor-2. Cancer Res 2001;61:6624–8.
19. Bello L, et al. Combinatorial administration of molecules that simultaneously inhibit angiogenesis and invasion leads to increased therapeutic efficacy in mouse models of malignant glioma. Clin Cancer Res 2004;10:4527–37.
20. Madsen SJ, et al. Photodynamic therapy of newly implanted glioma cells in the rat brain. Lasers Surg Med 2006;38:540–8.
21. Lamszus K, Kunkel P, Westphal M. Invasion as limitation to anti-angiogenic glioma therapy. Acta Neurochir Suppl 2003;88:169–77.
22. Friedl P, Wolf K. Tumor cell invasion and migration: diversity and escape mechanisms. Nat Rev Cancer 2003; 3:362–74.
23. Debnath J, Brugge J. Modelling glandular epithelial cancers in three-dimensional cultures. Nat Rev Cancer 2005;5:675–88.
24. Maher EA, et al. Malignant glioma: genetics and biology of a grave matter. Genes Dev 2001;15:1311–33.
25. Benjamin R, Capparella J, Brown A. Classification of glioblastoma multiforme in adults by molecular genetics. Cancer J 2003;9:82–90.
26. Merlo A. Genes and pathways driving glioblastomas in humans and murine disease models. Neurosurg Rev 2003;26:145–58.
27. Lal A, et al. Mutant epidermal growth factor receptor up-regulates molecular effectors of tumor invasion. Cancer Res 2002;62:3335–9.
28. Nishikawa R, et al. A mutant epidermal growth factor receptor common in human glioma confers enhanced tumorigenicity. Proc Natl Acad Sci U S A 1994;91:7727–31.
29. Nagane M, Levitzki A, Gazit A, Cavenee WK, Huang HJS. Drug resistance of human glioblastoma cells conferred by a tumor-specific mutant epidermal growth factor receptor through modulation of Bcl-X L and caspase-3-like proteases. Proc Natl Acad Sci U S A 1998; 95:5724–9.
30. Zhang L, Athale CA, Deisboeck TS. Development of a three-dimensional multiscale agent-based tumor model: simulating gene-protein interaction profiles, cell phenotypes and multicellular patterns in brain cancer. J Theor Biol 2007;244:96–107.
31. Stein AM, Demuth T, Mobley D, Berens M, Sander LM. A mathematical model of glioblastoma tumor spheroid invasion in a three-dimensional *in vitro* experiment. Biophys J 2007;92:356–65.
32. Athale CA, Deisboeck TS. The effects of EGF-receptor density on multiscale tumor growth patterns. J Theor Biol 2006;238:771–9.
33. Anderson ARA, Weaver AM, Cummings PT, Quaranta V. Tumor morphology and phenotypic evolution driven by selective presure from the microenvironment. Cell 2006;127:905–15.
34. Tysnes BB, Mahesparan R. Biological mechanisms of glioma invasion and potential therapeutic targets. J Neurooncol 2001;53:129–47.
35. Ishii N, et al. Frequent co-alterations of TP53, p16/CDKN2A, p14ARF, PTEN tumor suppressor genes in human glioma cell lines. Brain Pathol 1999;9:469–79.
36. Jensen RL. Hypoxia in the tumorigenesis of gliomas and as a potential target for therapeutic measures. Neurosurg Focus 2006;20:E24.
37. Chaplain MAJ. Avascular growth, angiogenesis and vascular growth in solid tumours: the mathematical modelling of the stages of tumour development. Math Comput Model 1996;23:47–87.
38. Bartels U, et al. Vascularity and angiogenesis as predictors of growth in optic pathway/hypothalamic gliomas. J Neurosurg 2006;104:314–20.
39. Preusser M, et al. Histopathologic assessment of hotspot microvessel density and vascular patterns in glioblastoma: poor observer agreement limits clinical utility as prognostic factors: a translational research project of the European Organization for Research and Treatment of Cancer Brain Tumor Group. Cancer 2006;107:162–70.
40. Macklin P, Lowengrub JS. Nonlinear simulation of the effect of microenvironment on tumor growth. J Theor Biol 2007;245:677–704.
41. Okada Y, et al. Selection pressures of TP53 mutation and microenvironmental location influence epidermal growth factor receptor gene amplification in human glioblastomas. Cancer Res 2003;63:413–6.
42. Hu B, et al. Angiopoietin-2 induces human glioma invasion through the activation of matrix metalloprotease-2. Proc Natl Acad Sci U S A 2003;100:8904–9.
43. Plate KH, Risau W. Angiogenesis in malignant gliomas. Glia 1995;15:339–47.
44. Rong Y, Durden DL, Van Meir EG, Brat DJ. 'Pseudopalisading' necrosis in glioblastoma: a familiar morphologic feature that links vascular pathology, hypoxia, and angiogenesis. J Neuropathol Exp Neurol 2006;65:529–39.
45. Sierra A. Metastases and their microenvironments: linking pathogenesis and therapy. Drug Resist Updat 2005;8:247–57.
46. van Kempen LCLT, Ruiter DJ, van Muijen GNP, Coussens LM. The tumor microenvironment: a critical determinant of neoplastic evolution. Eur J Cell Biol 2003;82:539–48.
47. Sinek J, et al. Predicting drug pharmacokinetics and effect in vascularized tumors using computer simulation. J Math Biol 2009;58:485–510.
48. Jain RK. Normalizing tumor vasculature with anti-angiogenic therapy: a new paradigm for combination therapy. Nat Med 2001;7:987–9.
49. Ferrari M. Cancer nanotechnology: opportunities and challenges. Nat Rev Cancer 2005;5:161–71.
50. Kenny PA, Lee GY, Bissell MJ. Targeting the tumor microenvironment. Front Biosci 2007;12:3468–74.

Cancer Research
The Journal of Cancer Research (1916–1930) | The American Journal of Cancer (1931–1940)

AACR American Association for Cancer Research

Multiparameter Computational Modeling of Tumor Invasion

Elaine L. Bearer, John S. Lowengrub, Hermann B. Frieboes, et al.

Cancer Res 2009;69:4493-4501. Published OnlineFirst April 14, 2009.